ChanEst Dataset: A Reconfigurable Framework and Benchmark for Deep Learning–Based 6G Channel Estimation

OKOYEIGBO, Obinna <http://orcid.org/0000-0003-4546-4127>, DENG, Xutao <http://orcid.org/0000-0002-7372-3758>, SHERIFF, Ray <http://orcid.org/0000-0003-4143-692X>, JEREMIAH, Daniel <http://orcid.org/0009-0000-0649-6324> and SHOBAYO, Olamilekan <http://orcid.org/0000-0001-5889-7082>

telecom

MDPI

Article

ChanEst Dataset: A Reconfigurable Framework and Benchmark for Deep Learning–Based 6G Channel Estimation

Obinna Okoyeigbo [1,*], Xutao Deng [1], Ray Sheriff [1], Daniel Jeremiah [2] and Olamilekan Shobayo [3]

[1] Department of Engineering, Edge Hill University, Ormskirk, Lancashire L39 4QP, UK; dengx@edgehill.ac.uk (X.D.); sheriffr@edgehill.ac.uk (R.S.)
[2] Department of Computer Science, Asia Pacific University of Technology and Innovation, Kuala Lumpur 57000, Malaysia; tp091738@mail.apu.edu.my
[3] School of Computing and Digital Technologies, Sheffield Hallam University, Sheffield S1 2NU, UK; o.shobayo@shu.ac.uk
* Correspondence: obinna.okoyeigbo@edgehill.ac.uk

Abstract

Accurate channel estimation is essential for reliable wireless communication, yet it becomes significantly challenging in 6G due to extreme propagation conditions. Factors such as high mobility, large delay spreads, and low signal-to-noise ratios (SNRs) create environments where traditional estimators struggle to perform effectively. While deep learning (DL)–based channel estimation has emerged as an alternative approach, its advancement is hindered by the lack of standardized and reproducible datasets that follow 3GPP-compliant signal models and realistic receiver preprocessing. This paper introduces ChanEst, a reproducible dataset generation framework for DL-based channel estimation. The ChanEst dataset uses 3GPP-compliant physical-layer procedures, demodulation reference signals (DMRS), tapped delay line (TDL) channel models, and FR3 (Frequency Range 3) configurations, performing stratified random sampling of key channel parameters to ensure statistical diversity. Least squares (LS) estimates are obtained and interpolated across the time–frequency grid to construct practical receiver input tensors, while the corresponding labels are derived from the perfect channel responses produced by the channel model. The resulting datasets are stored as real-valued tensors suitable for DL models and accompanied by metadata logs to enable stratified evaluation and fair benchmarking. Comprehensive statistical analysis validates the dataset's diversity and physical consistency, and a fully implemented DL baseline model demonstrates its practical machine learning utility by outperforming conventional estimators under severe channel impairments. The ChanEst dataset is publicly available on Mendeley Data, with full code provided on GitHub, enabling reproducible experimentation for DL-based 6G channel estimation.

Keywords: 5G/6G wireless communication; deep learning; channel estimation; OFDM; dataset generation; benchmark; FR3; TDL channel model; Doppler shift; delay spread

Received: 1 March 2026
Revised: 14 April 2026
Accepted: 19 May 2026
Published: 1 June 2026

1. Introduction

The next-generation (6G and beyond) wireless systems are expected to push beyond 5G capabilities in terms of capacity, latency, reliability, and connectivity density, while supporting new use cases such as immersive communications, sensing integration, and highly mobile connectivity. These targets imply operation under extreme propagation conditions, including high mobility, strong time variation, and frequency-selective multipath, which collectively make accurate channel state information (CSI) increasingly difficult to

acquire and maintain [1]. In multicarrier systems, CSI quality directly impacts equalization, demodulation, link adaptation, and ultimately end-to-end reliability and spectral efficiency.

Channel estimation becomes particularly challenging in 6G due to the combined effects of large delay spreads, severe Doppler shifts, and low signal-to-noise ratios (SNRs). Conventional estimators such as least squares (LS) and minimum mean square error (MMSE) are well-studied and have been widely adopted in previous-generation networks; however, their performance and robustness can degrade under high mobility, wideband frequency selectivity, and complex propagation conditions anticipated in future 6G networks. These effects motivate complementary approaches that can better exploit structure in the time–frequency channel response and remain robust across heterogeneous propagation conditions.

1.1. Deep Learning for Channel Estimation

Deep learning (DL) has emerged as a promising tool for channel estimation because it can learn complex nonlinear mappings directly from data, potentially capturing impairments and channel behaviors that are difficult to model analytically, thereby outperforming conventional estimators in challenging scenarios. Recent studies demonstrate the potential of convolutional neural networks (CNNs) and related architectures to improve estimation accuracy, particularly under low-SNR and high-mobility environments [2,3].

Beyond CNN-based models, recent research has also explored deeper architectures such as residual networks and hybrid model-driven approaches that combine traditional estimators with learned refinement stages [4,5]. These architectures aim to exploit the spatial and temporal structure of wireless channel responses and improve robustness in highly dynamic propagation conditions.

More broadly, existing studies and surveys consistently identify deep learning as a strong enabler for physical-layer design, highlighting its ability to learn compact channel representations and support data-driven, end-to-end optimization of wireless communication systems [6]. However, DL-based estimators are inherently data-driven. Their performance, generalization, and reproducibility depend strongly on the quality, diversity, and realism of the training/evaluation data. As a result, the availability of representative, standardized datasets remains a practical bottleneck, especially when the goal is fair benchmarking across models and against conventional baselines [7].

1.2. Existing Datasets and Limitations

Despite growing interest in DL-based channel estimation, public datasets explicitly designed for channel estimation under standardized 3GPP technical specifications and procedures remain relatively limited, and many studies still rely on internally generated datasets. This limits reproducibility and complicates fair, cross-paper comparisons, especially when training data distributions, receiver preprocessing, and label definitions differ across implementations. This broader need for open datasets, complete metadata, and transparent evaluation protocols is increasingly emphasized in the wireless-ML literature [8].

Many published deep learning-based channel estimators are trained on internally generated data with limited diversity, incomplete documentation, or non-released pipelines, further restricting reproducibility and fair benchmarking [9]. Recent efforts toward benchmark-oriented Orthogonal Frequency Division Multiplexing (OFDM) channel estimation also highlight the need for standardized comparisons and transparent dataset definitions. Furthermore, the requirements of next-generation networks motivate stressing estimators across joint extremes of low SNR, high Doppler, and large delay spread, which are often underrepresented in public datasets [10,11].

This emphasis on unified benchmarking across channel models and operating regimes (e.g., SNR and Doppler) is also reflected in recent published comparative/benchmark studies [12]. In addition, ongoing 6G discussions around the upper mid-band (often referred to as FR3, roughly 7–24 GHz) highlight the need to evaluate channel estimators under joint delay–Doppler–SNR stress, since this band offers increased bandwidth while retaining more favorable propagation characteristics than mmWave [13].

Publicly available wireless ML datasets have greatly improved reproducibility for tasks such as beam prediction/beam selection, particularly in geometry-based mmWave and massive-MIMO systems. For example, DeepMIMO [14] provides a ray-tracing-based dataset widely used for learning-based beam prediction and related problems, while Raymobtime and Raymobtime2 [15] have been introduced and used extensively for beam selection under mobility. While highly valuable for benchmarking, these datasets do not necessarily provide a reconfigurable end-to-end 3GPP-standardized pilot-aided channel-estimation pipeline (DM-RS insertion, pilot extraction/estimation, TF interpolation) paired with "perfect" supervision labels on the same time–frequency grid. As a result, researchers aiming to study standardized pilot-aided channel estimation often still need to implement their own end-to-end waveform generation, receiver preprocessing, and label extraction, which reduces comparability across works. This is specifically challenging for channel estimation because seemingly small differences in pilot placement, preprocessing, or label construction can substantially change reported performance [16,17].

Another limitation is reproducibility and reconfigurability. Many released datasets are distributed as fixed sample collections, lacking an openly documented generation pipeline and complete configuration metadata, which precludes regeneration, targeted extension, and systematic validation or stress testing. Furthermore, released datasets are often tied to a specific study configuration, such as fixed numerology, pilot pattern, or receiver preprocessing, making it difficult to produce matched variants for controlled comparisons [18]. Consequently, common research needs (e.g., scaling from SISO to MIMO, modifying numerology or pilot density, resizing the dataset for computational studies, or deliberately synthesizing extreme regimes) typically require re-implementing the entire pipeline, undermining comparability and fairness in benchmarking [6,19].

In addition, several dataset releases and simulation pipelines are scenario or regime-specific (for example, limited mobility ranges, fixed delay profiles/spreads, or narrow SNR coverage). While useful for initial investigations, such constraints may underrepresent the combined delay–Doppler–SNR stresses anticipated in 6G deployments [20]. Relatedly, some datasets are generated under simplified channel assumptions or narrow parameter ranges (e.g., reduced frequency selectivity or limited multipath diversity). While these assumptions simplify analysis, they may underrepresent the strong time–frequency selectivity experienced by wideband OFDM systems under large delay spreads and high mobility. These conditions are central to next-generation networks, and underrepresenting them limits the ability to develop and benchmark models intended for realistic 6G operating scenarios [21].

Finally, survey and benchmark-oriented studies repeatedly highlight that inadequate dataset documentation, limited metadata, inconsistent evaluation practices, and poor reproducibility remain major barriers to the reliable assessment of machine learning and deep learning physical-layer methods [7]. These works underscore the need for standardized, well-documented, and fully reproducible datasets [22]. Motivated by these gaps, ChanEst [23] is designed as a reproducible and reconfigurable dataset-generation framework that adheres to 3GPP standardized channel estimation procedures and spans a broad range of operating conditions, while providing detailed metadata to enable stratified and fair evaluation [24].

1.3. Motivation and Contributions

To address the above-mentioned limitations, this paper introduces the ChanEst dataset, a reproducible and reconfigurable dataset generation framework aligned with 3GPP physical-layer procedures. Unlike static datasets tied to fixed simulation settings, ChanEst provides an end-to-end, transparent, and regenerable pipeline that ensures methodological consistency across system configurations [25].

To capture 6G-relevant variability, the framework implements stratified randomization over 3GPP TDL channel profiles (TR 38.901) [25], SNR, delay spread, and Doppler shift, generating statistically diverse propagation conditions rather than narrow operating points. This enables robust training and fair evaluation across heterogeneous scenarios.

A central contribution is the definition of a receiver-realistic input–label pairing. Practical channel inputs are constructed via DM-RS extraction, LS estimation, and 2D time–frequency interpolation, producing noisy dense grids representative of real receiver observations. These are paired with perfectly matched OFDM-grid channel responses derived from the underlying channel model, ensuring consistent and physically grounded supervision.

Beyond the reference dataset, ChanEst enables scalable regeneration under varying antenna configurations (SISO/MIMO), subcarrier spacing, grid dimensions, and extreme propagation regimes while preserving the same preprocessing and labeling methodology. The dataset is released in MATLAB and HDF5 formats, together with structured metadata logs to support stratified performance analysis. To explicitly validate the dataset's utility for machine learning research, we further provide a fully evaluated deep learning baseline to serve as a reproducible benchmark.

The key contributions are summarized as follows:

- **Standard-compliant pipeline:** ChanEst integrates 3GPP-compliant DM-RS procedures and TDL channel models, providing realistic propagation characteristics aligned with widely used wireless system evaluation standards.
- **Receiver-realistic input representation:** The learning inputs are constructed from LS estimates followed by 2-D time–frequency interpolation, closely reflecting practical receiver processing rather than idealized channel observations.
- **Stratified sampling of propagation conditions:** Channel parameters such as SNR, delay spread, and Doppler shift are generated using stratified random sampling, ensuring balanced/uniform coverage of both typical and extreme propagation regimes.
- **Reproducible and reconfigurable framework:** Unlike existing datasets released as fixed collections of samples, ChanEst provides a fully reproducible generation pipeline with configurable parameters, allowing researchers to regenerate or extend the dataset under different configurations while preserving methodological consistency.
- **Validated deep learning benchmark:** To demonstrate practical deep learning utility, the ChanEst dataset is accompanied by a baseline model, providing researchers with a standardized starting point for developing and evaluating advanced architectures.

2. System Model and Receiver Preprocessing

This section describes the system model, pilot structure, modulation scheme, channel model, and noise assumptions used in the generation of the ChanEst dataset for deep learning–based channel estimation. A block diagram representing the system model is given in Figure 1.

Unless otherwise stated, the reference dataset configuration corresponds to a single-user SISO downlink OFDM system employing 3GPP TDL channel models, which capture multipath fading conditions representative of both line-of-sight (LOS) and non-line-of-sight (NLOS) propagation scenarios.

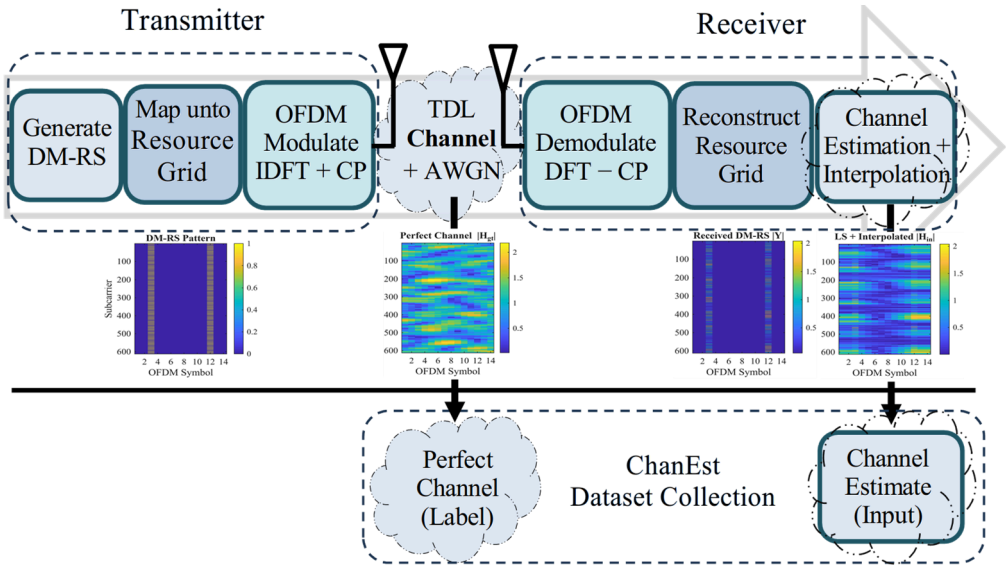

Figure 1. System model block diagram of the ChanEst dataset generation framework.

While simulation-based datasets cannot fully capture the complexity of real-world propagation environments, 3GPP TDL channel models provide widely accepted statistical representations of wireless channels and are commonly used for system-level evaluation and algorithm benchmarking.

2.1. OFDM Model

We consider an OFDM system over a frequency-selective fading channel. The OFDM frame is represented as a two-dimensional time–frequency resource grid comprising K subcarriers and L OFDM symbols per slot. Each resource element (RE) on the grid corresponds to one complex-valued modulation symbol. Let $X(k,n)$ denote the transmitted symbol on the subcarrier $k \in \{0,\ldots,K-1\}$ and OFDM symbol $n \in \{0,\ldots,L-1\}$. After OFDM modulation, cyclic prefix insertion, and transmission through the wireless channel, the received signal is OFDM-demodulated at the receiver, yielding the received resource grid $Y(k,n)$, which is expressed as:

$$Y(k,n) = H(k,n)X(k,n) + W(k,n), \tag{1}$$

where $H(k,n)$ is the channel frequency response on the OFDM grid and $W(k,n)$ is additive noise.

For MIMO configurations, the same model applies per transmit–receive antenna pair, and the channel response can be indexed as $H_{r,t}(k,n)$ for the receive antenna r and transmit antenna t.

2.2. Demodulation Reference Signal (DM-RS) Model

Channel estimation is pilot-aided using demodulation reference signals (DM-RS), inserted at predefined time–frequency locations. For standard compliance, the DM-RS structure and resource mapping follow 3GPP TS 38.211 [26], the PDSCH/DM-RS configuration is parameterized using TS 38.214 [27], and the propagation channel is generated using the 3GPP TDL models specified in TR 38.901 [25]. Let $\mathcal{P} \subset \{(k,n)\}$ denote the set of RE indices occupied by DM-RS. At $(k,n) \in \mathcal{P}$, the transmitted pilot symbol $X_p(k,n)$ is known at the receiver, giving the received pilot

$$Y_p(k,n) = H(k,n)\ X_p(k,n) + W(k,n),\ (k,n) \in \mathcal{P}. \tag{2}$$

In the default ChanEst configuration, the DM-RS pattern follows the Type-2 arrangement with 408 unique DM-RS REs per slot, per port/layer, over a $K \times L = 612 \times 14$ time–frequency grid (i.e., 8568 REs per slot) as shown in Figure 2. This corresponds to a pilot density of 4.76% (408/8568), providing a realistic pilot overhead consistent with practical receiver operation. In ChanEst, DM-RS indices and symbols are generated directly from the configured PDSCH/DM-RS settings, ensuring that the pilot set is fully determined by standard-aligned parameters and is consistent with the assumptions of a practical receiver.

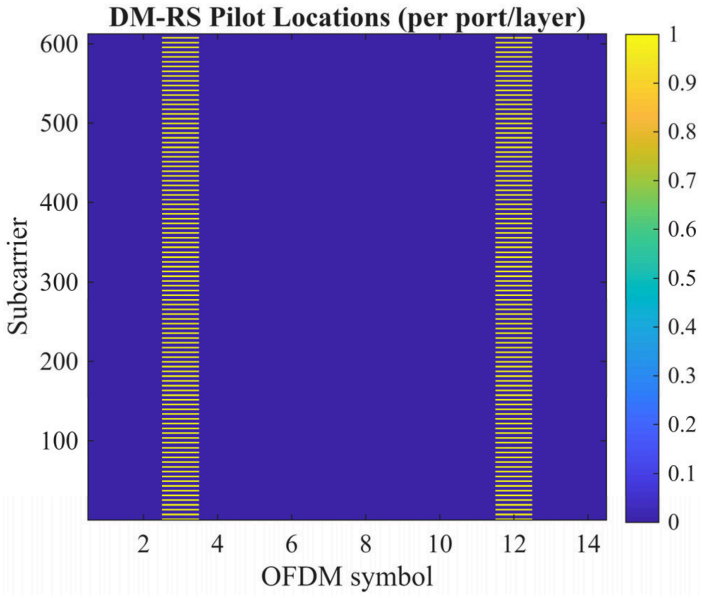

Figure 2. Time–frequency resource grid showing DM-RS (Type-2) pilot locations.

2.3. Channel Model and Scenario Randomization

The wireless channel is modeled using 3GPP-compliant TDL channels as specified in TR 38.901 [25]. The corresponding time-varying channel impulse response is

$$h(t,\tau) = \sum_{\ell=1}^{L_p} \alpha_\ell(t)\, \delta(\tau - \tau_\ell), \tag{3}$$

where L_p is the number of multipath components, $\alpha_\ell(t)$ is the time-varying complex gain of path ℓ, and τ_ℓ is the corresponding delay. The frequency-domain channel response $H(k,n)$ is obtained by applying the Fourier transform of the impulse response on the OFDM grid.

To ensure balanced coverage of propagation conditions, channel parameters are generated using stratified random sampling within predefined configurable ranges. Random jitter is then applied within each stratum, and independent random permutations are used across parameters to avoid artificial correlations between SNR, delay spread, and Doppler. In addition, TDL profile types are assigned using balanced sampling to ensure equal representation of different multipath environments across the dataset.

The framework supports two equivalent modes for time selectivity. In Doppler-driven mode, the maximum Doppler shift f_D is sampled directly (5 to 5000 Hz) and applied to the TDL channel realization. An equivalent speed is then computed as $v_{\text{eq}} = \frac{c\, f_D}{f_c}$, where c is the speed of light, f_c is the carrier frequency. Here, $f_c = 7$ GHz is set in the upper mid-band (often referred to as FR3), which has been widely discussed for 6G as a spectrum region offering a practical balance between propagation characteristics and contiguous bandwidth availability [10,28].

2.4. Noise Model

The received signal is corrupted by noise samples $W(k,n)$, modeled as independent and identically distributed complex Gaussian random variables with zero mean and variance σ^2:

$$W(k,n) \sim \mathcal{CN}\left(0,\sigma^2\right). \tag{4}$$

The noise variance σ^2 is determined by the selected SNR, which is randomized over a predefined range to promote diversity.

2.5. Learning Input (Interpolated LS)

At the receiver, an initial estimate of the channel is obtained at DM-RS locations using a least-squares (LS) estimator:

$$\hat{H}_{\mathrm{LS}}(k,n) = \frac{Y_p(k,n)}{X_p(k,n)}, (k,n) \in \mathcal{P}. \tag{5}$$

The LS estimator is computationally efficient; however, it is sensitive to noise and provides channel estimates only at sparse pilot locations $\mathcal{P}$.

Since DM-RS occupy only a subset of the full resource grid, a dense estimate is constructed by applying a two-dimensional interpolation operator across frequency and time:

$$\hat{H}_{\mathrm{in}}(k,n) = \mathcal{I}\left(\hat{H}_{\mathrm{LS}}(k,n)\right),\ \forall (k,n) \in \{0,\ldots,K-1\} \times \{0,\ldots,L-1\}. \tag{6}$$

Linear interpolation is employed due to its low complexity and common use in practical receivers. Importantly, the resulting interpolated channel estimate $\hat{H}_{\mathrm{in}}$ is used as the learning input, not as the final estimator output.

2.6. Ground-Truth Label (Perfect Channel)

Supervised learning requires ground-truth labels aligned to the same grid as the inputs. For each sample, the generator obtains the perfect channel frequency response on the OFDM grid, $H_{\mathrm{gt}}(k,n)$, directly from the channel model for the given realization. This provides a consistent target for learning and ensures input–label pairs are synchronized in time–frequency. The network is trained to map the interpolated pilot-based estimate $\hat{H}_{\mathrm{in}}$ to the ideal grid-aligned channel H_{gt}.

2.7. Real-Valued Tensor Representation

Although the channel inputs and labels are complex-valued, most DL frameworks operate on real-valued tensors. Therefore, the inputs and labels are decomposed into real and imaginary components and stacked along the channel C dimension, to preserve the full complex information. For SISO, this yields tensors of size $K \times L \times C$, where $C = 2$ (real and imaginary). For MIMO, channels are packed across antenna links, leading to $C = 2 \times N_{\mathrm{Tx}} \times N_{\mathrm{Rx}}$, where N_{Tx} and N_{Rx} are the numbers of transmit and receive antennas, respectively. A simplified 3×3 complex-valued grid is decomposed as:

$$\text{Complex-valued } 3 \times 3 \text{ grid}: \begin{bmatrix} 0.73+0.12\mathrm{j} & -0.41+0.66\mathrm{j} & 0.85-0.32\mathrm{j} \\ 0.45+0.28\mathrm{j} & 0.21-0.52\mathrm{j} & -0.64+0.75\mathrm{j} \\ -0.58+0.41\mathrm{j} & 0.79-0.13\mathrm{j} & 0.33+0.57\mathrm{j} \end{bmatrix}$$

$$\text{Real component}: \begin{bmatrix} 0.73 & -0.41 & 0.85 \\ 0.45 & 0.21 & -0.64 \\ -0.58 & 0.79 & 0.33 \end{bmatrix}$$

$$\text{Imaginary component}: \begin{bmatrix} 0.12 & 0.66 & -0.32 \\ 0.28 & -0.52 & 0.75 \\ 0.41 & -0.13 & 0.57 \end{bmatrix}$$

The dataset stores raw input and labels; normalization can be applied by the user during training if desired. For example, per-sample RMS normalization may be applied to the input (and/or label) tensors to stabilize optimization, provided the same convention is used consistently across training and evaluation.

3. Dataset Generation and Reconfigurable Framework

Using the system model above, the ChanEst dataset is generated by repeatedly simulating independent channel realizations under randomized propagation conditions and applying a receiver-aligned pilot-aided estimation pipeline. A defining feature of ChanEst is its reconfigurable generator design: the same pipeline can be re-instantiated under different system settings without altering the methodological core, thereby supporting different antenna orders (SISO/MIMO), dataset sizes, grid/numerology settings, DM-RS configurations, and sampling strategies (typical vs. extreme regimes). Hence, ChanEst is not merely a fixed dataset dump, but a reproducible generation framework that can be adapted to new research questions while maintaining a consistent and comparable pipeline.

3.1. Configurable Parameters

Table 1 summarizes the default configuration used in this release and highlights parameters that are directly reconfigurable in the generator. When configuration settings change (e.g., antenna order or grid size), derived quantities such as packed channels $C = 2N_{\mathrm{Tx}}N_{\mathrm{Rx}}$ and tensor dimensions update automatically.

Table 1. ChanEst dataset configuration and reconfigurable parameters.

Block	Parameter	Default (This Dataset)
Dataset	Number of samples (N)	10,000
	Sampling	Stratified
Antenna	$N_{Tx} \times N_{Rx}$	1×1 (2×2, 4×4 if MIMO)
	Packed channels ($C = 2 \times N_{Tx} \times N_{Rx}$)	2
NR Grid	Subcarriers (K)	612
	OFDM symbols (L)	14
	Subcarrier spacing (Δf)	60 kHz
DM-RS	DM-RS type	Type 2
	Layers (N_{layers})	N_{Tx}
	CDM lengths $\left[\ell_f, \ell_t\right]$	[2, 1]
	Pilot density	4.76% (408/8568) REs per slot, per layer
Channel	Model	3GPP TDL Channel
	Delay profiles	TDL-A to TDL-E
	Delay spread range	10–2000 ns
	Doppler range	5–5000 Hz

Table 1. *Cont.*

Block	Parameter	Default (This Dataset)
	Carrier frequency f_c	7 GHz (FR3)
	MIMO correlation	Low/Medium/High
Noise	SNR range	-10 to 30 dB
Input/Output	Input ($\hat{H}_{\text{in}}$)	DM-RS LS/CDM (if MIMO) + 2D interpolation
	Label (H_{gt})	Perfect OFDM-response
	Tensor size	$612 \times 14 \times C \times N$

The default delay spread range (10–2000 ns) spans short-delay indoor multipath to highly dispersive wide-area channels, while the Doppler range (5–5000 Hz) at $f_c = 7$ GHz corresponds to approximately 0.2–214 m/s (about 0.7–770 km/h), covering pedestrian mobility to high-mobility scenarios. The SNR range (-10 to 30 dB) includes noise/interference-limited conditions as well as high-SNR conditions. If a different deployment scenario is targeted, these ranges are reconfigurable in the generator, enabling regeneration of scenario-specific datasets under the same standardized pipeline and aligned input–label definition.

To ensure broad coverage, the generator supports stratified sampling over SNR/delay/Doppler bins, avoiding concentration in a narrow operating regime. Optionally, the framework can emphasize extreme conditions (e.g., low SNR, high Doppler, large delay spread) via targeted oversampling to support stress testing and benchmarking in challenging 6G-relevant regimes.

3.2. ChanEst Generation Procedure

ChanEst dataset is implemented in MATLAB (R2025a) using the 6G Exploration Library, ensuring standard-compliant waveform generation, DM-RS, and TDL channel modeling functions. Algorithm 1 summarizes the end-to-end ChanEst dataset generation pipeline. For each sample, DM-RS are inserted into an OFDM grid, transmitted through a randomized TDL channel realization, corrupted by additive white Gaussian noise (AWGN) at a randomized SNR, and processed by a receiver pipeline that extracts pilots, forms LS estimates, and performs 2D interpolation to generate dense-grid learning inputs. Perfect OFDM-grid channel responses are saved as labels. Scenario logs and metadata are recorded for reproducibility and stratified evaluation.

3.3. Dataset Contents and Usage

The ChanEst dataset release includes four main components:

3.3.1. Input Tensor *X_input*

A dense interpolated LS channel estimate on the OFDM grid, packed into real and imaginary components and extended across MIMO links where applicable.

3.3.2. Label Tensor *Y_label*

The corresponding perfect OFDM-grid channel response, packed using the same real and imaginary representation for consistency.

3.3.3. Per-Sample Logs

Metadata describing SNR, delay spread, Doppler shift, user speed (calculated), TDL profile, and (for MIMO) correlation settings.

Algorithm 1: ChanEst Dataset Generation for Deep Learning-Based Channel Estimation

Input: Simulation parameters: delay profiles, Doppler, delay spread, dataset size N, SNR range, subcarrier spacing, grid size, antenna configuration (N_{Tx}, N_{Rx}), DM-RS configuration.

Output: Dataset comprising input tensor $\hat{H}_{\text{in}}$ (interpolated LS estimate), label H_{gt} (perfect OFDM channel), and metadata logs (SNR, delay spread, Doppler, TDL profile, correlation).

1: Initialize system parameters (subcarrier spacing, number of resource blocks, grid size $K \times L$, cyclic prefix, antenna configuration, modulation scheme).
2: Configure PDSCH, generate DM-RS symbols and indices using standard-compliant waveforms and functions in MATLAB's 6G library.
3: Create resource grid and insert DM-RS according to the pilot pattern $\mathcal{P} \subset \{(k, n)\}$.
4: Perform OFDM modulation to generate transmit waveform $x(t)$.
5: Initialize 3GPP TDL channel model (N_{Tx}/N_{Rx}), sampling rate F_s, and ChannelResponseOutput = "OFDM-response", and compute padding length.
6: Perform stratified (or random) sampling for SNR, delay spread, Doppler shift/speed, delay profile and MIMO correlation (if applicable).
7: Pre-allocate memory for storing dataset (input: $\hat{H}_{\text{in}}$ and labels: H_{gt}); initialize metadata logs (SNR, delay spread, Doppler, speed, profile, seed, etc.).
8: **For** $i = 1, \ldots, N$:
  a: Set sample parameters (TDL profile, delay spread, Doppler/speed, SNR, seed, MIMO correlation) and record them in the metadata logs.
  b: Transmit waveform $x(t)$ through the channel to obtain the received wave form $y(t)$, together with the perfect channel response and timing offset.
  c: Add AWGN based on SNR; compensate timing offset; OFDM-demodulate.
  d: Estimate the channel at DM-RS positions using LS estimation and apply 2-D TF interpolation to obtain a full-grid estimate.
  e: Separate real and imaginary components of inputs and labels and stack them into channel dimensions $C = 2N_{Tx}N_{Rx}$, forming real-valued tensors.
  f: Store dataset: $X\_input(:,:,:,i) \leftarrow \hat{H}_{\text{in}}$ (packed), $Y\_label(:,:,:,i) \leftarrow H_{\text{gt}}$ (packed).
End For
9: Save dataset tensors, metadata logs, and configurations to enable full reproducibility.
10: Perform quick quality assurance: summary statistics of SNR, delay spread, Doppler shift, and simple correlation/NMSE (Normalized Mean Squared Error).
11: Output the final dataset as 4D tensors of size ($K \times L \times C \times N$) e.g., $612 \times 14 \times 2 \times 10$k.

3.3.4. Configuration Objects and Metadata

Detailed descriptions of numerology, pilot structure, and generation parameters used to produce each dataset instance.

To use the dataset, the input tensor *X_input* together with its corresponding label tensor *Y_label* are loaded and subsequently partitioned into training, validation, and test sets. The accompanying metadata (such as SNR, delay spread, Doppler shift, and TDL profile) may be employed to stratify these splits or to benchmark model performance across distinct propagation regimes. The tensors are provided without amplitude normalization to preserve their physical scaling; however, when normalization is required for training stability, a clearly defined per-sample convention (e.g., RMS normalization applied consistently to both inputs and labels) should be adopted and documented to maintain fairness in comparisons.

ChanEst supports multiple learning paradigms. In supervised learning, the model is trained to map the interpolated LS input estimates to the corresponding perfect channel

responses on the same time–frequency grid. The framework also facilitates unsupervised and self-supervised approaches, where labels may be omitted, and learning is guided by enforcing measurement consistency at pilot positions or by applying masked-reconstruction objectives directly on the time–frequency channel grid.

4. ChanEst Dataset Validation

This section provides confidence that the ChanEst dataset is suitable for training and for controlled, reproducible benchmarking. The ChanEst dataset is validated in terms of scenario coverage, input–label consistency, and physical plausibility. The validation combines summary statistics with visual analytics, including parameter histograms, input–label consistency distributions, binned NMSE trends, and qualitative visualizations illustrating the time–frequency structure of the wireless channel.

Table 2 summarizes the numerical statistics of the scenario parameters and, additionally, baseline input–label consistency metrics (correlation and NMSE) computed between the interpolated LS inputs and the corresponding perfect channel labels.

Table 2. Statistical summary of scenario parameters of ChanEst dataset.

Parameter	Mean	Std	Min	P5	P50	P95	Max
SNR (dB)	10.00	11.55	−10.00	−8.00	10.00	28.00	30.00
RMS Delay Spread (ns)	1005.00	574.49	10.07	109.41	1004.98	1900.48	1999.84
Max Doppler Shift (Hz)	2502.50	1442.00	5.36	254.68	2502.51	4750.24	4999.63
User Speed (m/s)	107.18	61.76	0.23	10.91	107.18	203.44	214.12
Correlation	0.75	0.21	0.00	0.34	0.80	0.98	1.00
NMSE (linear)	0.76	2.20	0.00	0.05	0.38	2.18	82.87
NMSE (dB)	−4.60	5.29	−37.83	−13.37	−4.25	3.39	19.18

4.1. Scenario Coverage and Statistics

Figure 3 illustrates the statistical coverage of the ChanEst dataset for the default configuration. The sampled SNR, delay spread, and Doppler shift are well distributed over their respective ranges, confirming controlled coverage of diverse propagation and noise conditions rather than concentration in a narrow operating scenario. The 3GPP TDL profiles (TDL-A to TDL-E) are also evenly represented, ensuring balanced multipath diversity across samples. For the default configuration, the DM-RS pilot density is 4.76% (408 unique DM-RS REs out of 8568 REs per slot, per port), providing a realistic pilot overhead consistent with practical pilot-aided estimation.

Together, these statistics validate that the dataset offers broad scenario coverage and avoids dominance by a single profile, mobility condition, or SNR regime. This diversity is essential for robust training and fair evaluation of data-driven channel estimators.

4.2. Input–Label Consistency

A core requirement for supervised learning is that the input $\hat{H}_{\text{in}}(k, n)$ remains physically consistent with the corresponding ground-truth label $H_{\text{gt}}(k, n)$ generated from the same channel realization. To verify this consistency, the correlation coefficient and NMSE between inputs and labels are evaluated across the dataset.

As shown in the correlation distribution in Figure 4a, most samples cluster at high correlation values, indicating that the input preserves the dominant channel structure under typical operating conditions. The lower-correlation tail captures more challenging scenarios (e.g., low SNR, high Doppler shift, and/or large delay spread), consistent with Table 2, and reflects expected limitations of sparse pilot observations and interpolation in severe conditions.

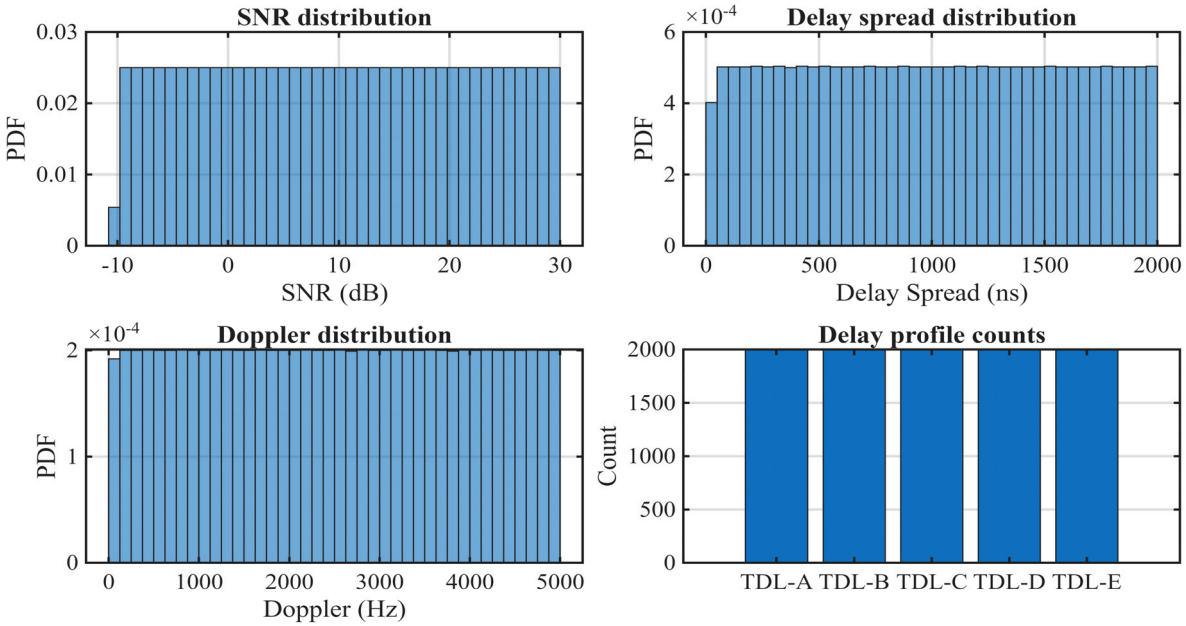

Figure 3. Statistical coverage of the ChanEst dataset, including distributions of SNR, delay spread, Doppler shift, and TDL profile counts.

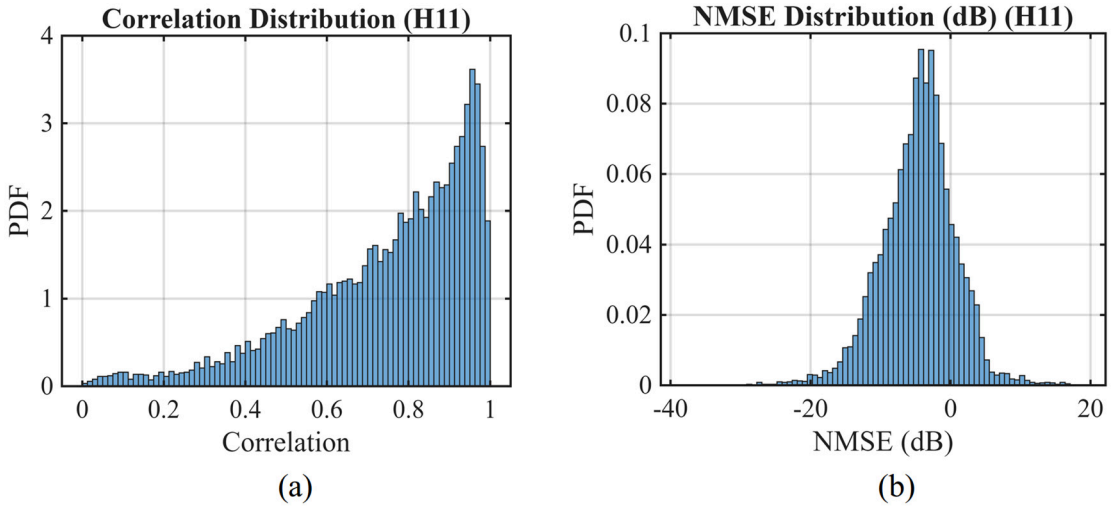

Figure 4. Input–label consistency metrics across the ChanEst dataset: (**a**) probability density function (PDF) of the correlation coefficient, and (**b**) PDF of the NMSE distribution.

The corresponding NMSE distribution in Figure 4b also confirms a broad spread of baseline pilot/interpolation error across ChanEst. Overall, these results validate the input–label pairing and demonstrate that the dataset spans both mild and extreme propagation conditions, supporting realistic benchmarking of learning-based channel estimation methods.

4.3. Channel Parameter Sensitivity

To verify that the ChanEst dataset varies meaningfully with the underlying propagation and noise conditions, NMSE trends are plotted by binning samples according to a scenario variable and computing the median and mean NMSE per bin (Figure 5). A clear decreasing trend is observed with increasing SNR, consistent with reduced noise corruption of DM-RS observations. Conversely, NMSE increases with RMS delay spread, as larger delay spreads increase frequency selectivity and reduce the ability of sparse pilots

to capture rapid subcarrier variation, thereby increasing interpolation mismatch. Finally, NMSE increases with maximum Doppler shift, reflecting stronger time selectivity: higher Doppler reduces temporal coherence across OFDM symbols, making interpolation less reliable and increasing baseline error.

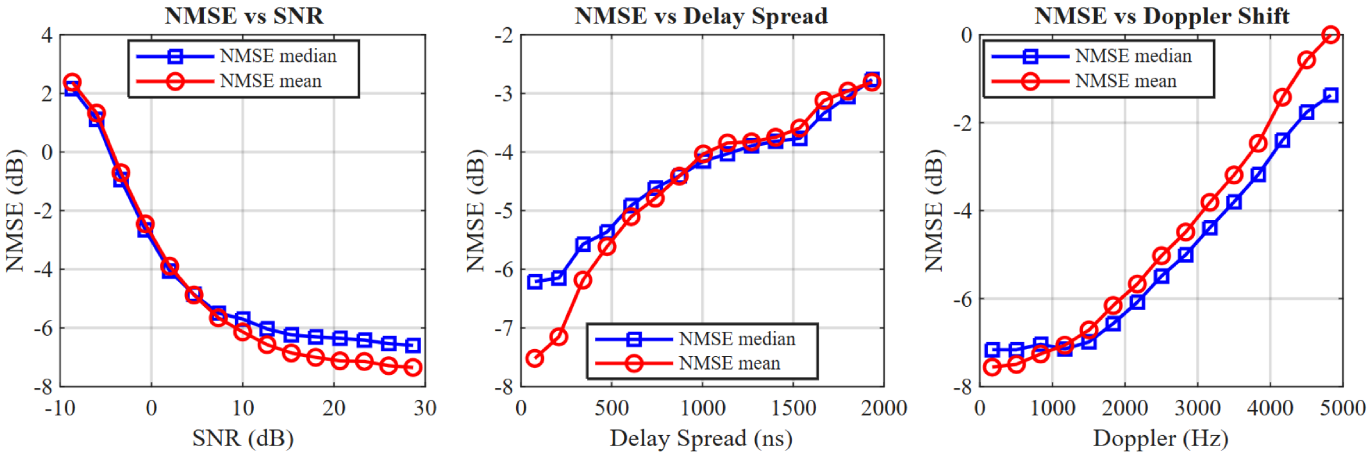

Figure 5. Median and mean NMSE as a function of SNR, delay spread, and Doppler shift.

Overall, these trends confirm physically consistent sensitivity to noise, delay, and mobility effects, and provide a reproducible baseline characterization of estimation difficulty for benchmarking data-driven estimators under controlled variations in SNR, delay spread, and Doppler shift.

4.4. Metadata Predictability and Importance

To further validate that ChanEst's estimation difficulty is determined by the underlying propagation and noise conditions, we assess whether the baseline estimation error can be predicted solely from the per-sample scenario metadata. This acts as a dataset-level sanity check, ensuring the relationship between propagation conditions and estimation performance is deterministic and physically sound.

Specifically, a regression model is trained to predict the True NMSE (dB) using only four features (SNR, delay spread, maximum Doppler shift, and TDL profile). Here, the True NMSE (dB) refers to the actual baseline estimation error computed between the input and the label, i.e., the NMSE evaluated directly from the channel tensors. The regression model therefore learns to predict this physically computed True NMSE using metadata features only, yielding the Predicted NMSE (dB), which is the metadata-based estimate of the true baseline error.

As shown in Figure 6a, the predicted NMSE closely tracks the true NMSE on the holdout test set, achieving a high coefficient of determination ($R^2 = 0.85$) and an RMSE of 2.08 dB. This confirms that approximately 85% of the variability in estimation difficulty is directly explainable by the provided metadata.

Figure 6b reports predictor importance. As expected, the SNR is the dominant contributor to NMSE variability. This is followed by Doppler shift, which quantifies time-selectivity, while delay spread and TDL profile provide additional explanatory power regarding frequency-selective fading. These results provide an additional dataset-level sanity check: (i) error trends are consistent and learnable from physical descriptors, and (ii) the released metadata logs are meaningful for stratified evaluation, controlled stress testing, and fair benchmarking across operating regimes.

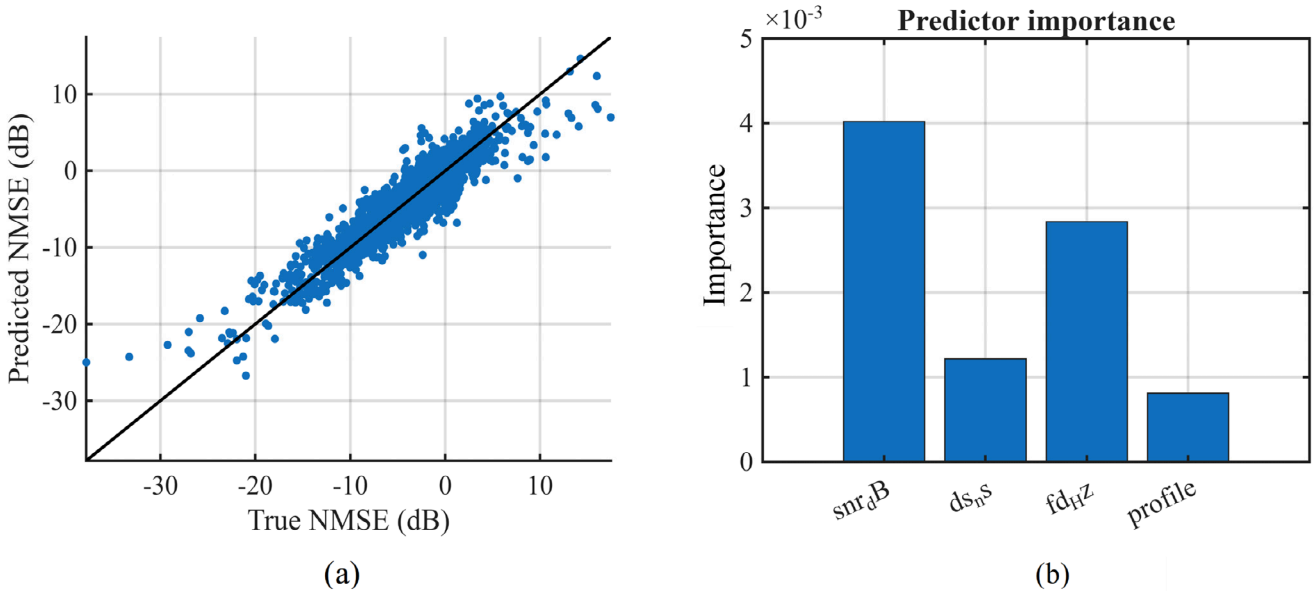

Figure 6. NMSE predictability from scenario metadata: (**a**) Predicted NMSE versus True NMSE (dB), and (**b**) corresponding predictor importance.

4.5. Channel Visualization

To qualitatively assess time–frequency structure in ChanEst, the channel magnitude $|H(k,n)|$ is visualized using 2-D heatmaps and 3-D surfaces (Figure 7). Heatmaps highlight frequency selectivity (variation across subcarriers) and time selectivity (variation across OFDM symbols), while direct comparison of $\hat{H}_{\text{in}}$ and H_{gt} for the same sample illustrates where pilot sparsity and interpolation smooth fine-scale structure. In a best-case example (high SNR, low Doppler, small delay spread), the input closely matches the label, whereas in a worst-case example (low SNR, high Doppler, large delay spread), the mismatch increases due to compounded noise, high mobility, and reduced coherence.

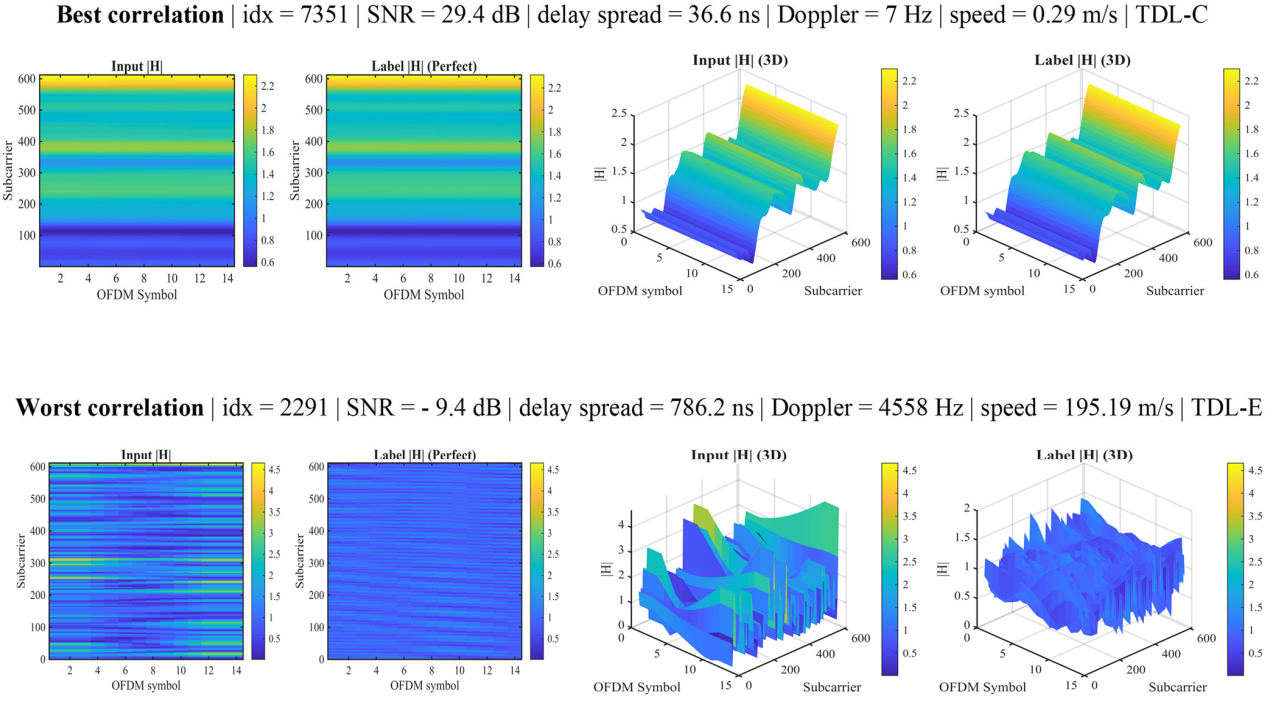

Figure 7. Two-dimensional heatmaps and 3D surfaces for best- and worst-case samples (input $\hat{H}_{in}$ and label H_{gt}), illustrating increased mismatch under low SNR, high Doppler, and large delay spread.

Plotting $|H(k, n)|$ as a 3-D surface provides an additional geometric interpretation of channel variability. Rotating the surface yields complementary views. The top-down view approximates the 2-D heatmap, side views emphasize ridge-like structures along time or frequency, and oblique views reveal localized peaks and sharp gradients that are less apparent in 2-D. These perspectives are useful for diagnosing difficult channel conditions associated with higher delay and Doppler selectivity.

5. Deep Learning Benchmark Evaluation

To address the practical utility of the ChanEst dataset, we evaluate a representative deep learning baseline model. This validates that the dataset effectively supports the training of data-driven estimators capable of mitigating severe propagation impairments with low SNR, large delay spreads, and high Doppler shifts, where traditional estimators fail.

5.1. Benchmark Deep Learning Architecture

We implemented a lightweight, fully convolutional neural network (CNN) formulated to map the noisy, interpolated LS channel estimates ($\hat{H}_{in}$) to the perfect ground-truth channel responses (H_{gt}). The network architecture and training hyperparameters are summarized in Table 3. The ChanEst dataset was partitioned into an 80% training set, a 10% validation set, and a 10% held-out test set. All benchmark performance metrics and visualizations were evaluated on the unseen test set to ensure a fair and unbiased assessment of the model's generalization capabilities.

Table 3. Baseline CNN architecture and training hyperparameters.

Component	Parameter/Layer Type	Details/Configuration
Input Layer	Image Input	Dimension: $K \times L \times 2$ (Real and Imaginary)
Hidden Layers	$3 \times$ Conv2D + ReLU	64 filters, 3×3 kernel, zero-padding ("same")
Output Layer	Conv2D	2 filters, 3×3 kernel, zero-padding ("same")
Loss Function	Regression	Mean Squared Error (MSE)
Hyperparameters	Optimizer	Adam
	Initial Learning Rate	1×10^{-3}
	Mini-Batch Size	16
	Max Epochs	20

5.2. Benchmark Performance Analysis

The MSE performance of the trained deep learning baseline is compared against the conventional LS estimator across varying propagation conditions, as presented in Figure 8. Additionally, the overall average performance metrics across the entire test set are summarized in Table 4, establishing the quantitative baseline scores for future benchmarking.

Table 4. Overall Benchmark Performance on the Test Set.

Metric	Conventional LS	DL Baseline	Performance Gain
Average NMSE (Linear)	0.8087	0.4822	–
Average NMSE (dB)	−0.92 dB	−3.17 dB	2.25 dB
Average MSE (Linear)	0.263	0.1702	
Average MSE (dB)	−5.80 dB	−7.69 dB	1.89 dB

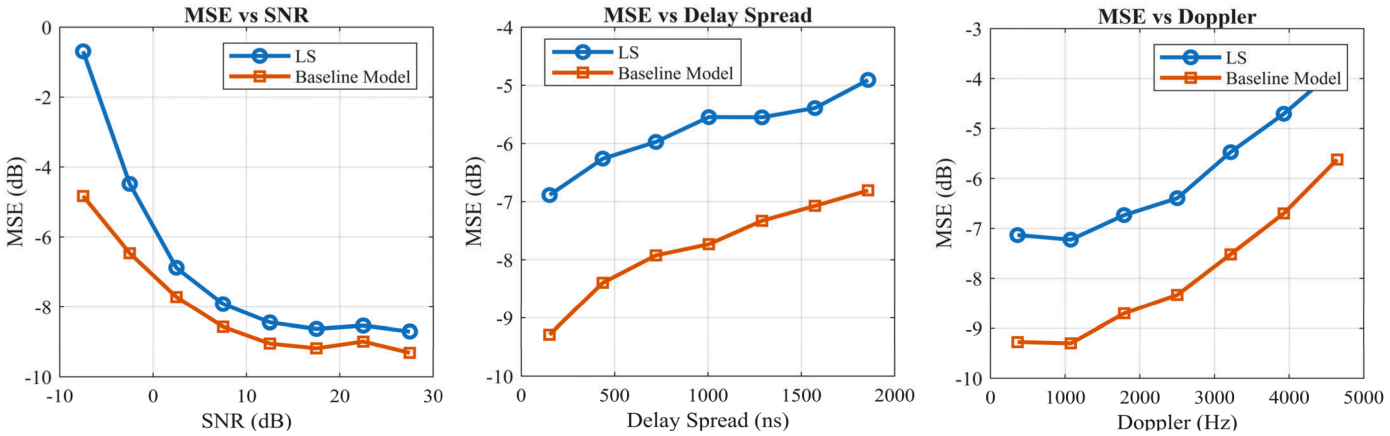

Figure 8. MSE (dB) performance comparison between the conventional LS estimator and the DL Baseline across varying SNR, Delay Spread, and Doppler conditions.

As illustrated in Figure 8 and Table 4, the lightweight deep learning baseline consistently outperforms the conventional LS estimator across all evaluated propagation regimes, yielding an overall average NMSE performance gain of 2.25 dB. While traditional estimators perform poorly in extreme 6G scenarios, the deep learning model acts as an effective learned denoiser under low SNR conditions and leverages spatial-frequency correlations to mitigate interpolation mismatch under large delay spreads (up to 2000 ns) and rapid temporal decorrelation (high Doppler shifts up to 5000 Hz).

Although performance inevitably degrades under joint extreme conditions, the CNN degrades much more gracefully than the LS baseline. This 2.25 dB improvement, achieved with a simple, shallow architecture, confirms the learnability of the dataset, while deliberately leaving significant room for future researchers to deploy more complex, state-of-the-art models (such as deep residual networks or transformers) to further close the performance gap in extreme 6G environments.

To complement these quantitative results, Figure 9 provides a qualitative visual comparison of the perfect ground-truth channel and the DL prediction for two representative test samples. The 2D heatmaps and 3D surfaces demonstrate that the model successfully reconstructs the fine-grained time–frequency structure of the channel, accurately capturing the complex signal peaks and valleys caused by multipath fading and mobility.

5.3. Implications for Deep Learning Research

These results confirm the practical machine learning value of the ChanEst dataset. The predictable and physically consistent improvement of the deep learning baseline over the conventional LS method proves that the dataset contains learnable, structured representations of complex 6G channel impairments. By releasing this validated deep learning baseline as part of the ChanEst codebase, researchers are provided with a standardized, reproducible starting point to benchmark more advanced SOTA architectures.

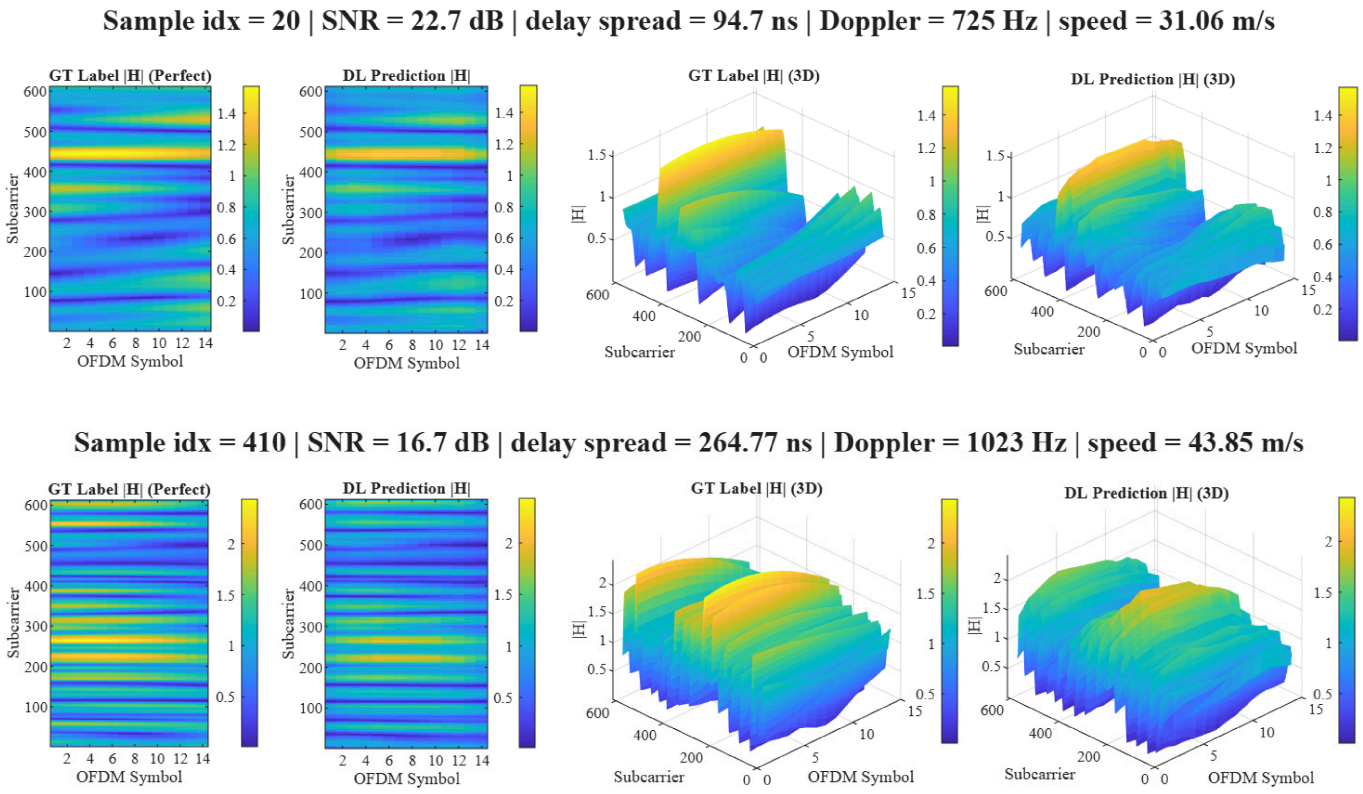

Figure 9. Qualitative visual comparison of the perfect ground-truth channel and the DL prediction across 2D heatmaps and 3D surfaces for two representative test samples.

6. Conclusions

This paper presented ChanEst, a reproducible and reconfigurable dataset generation framework for deep learning–based channel estimation. ChanEst employs standard-compliant physical-layer procedures and 3GPP TDL channel models to emulate realistic 6G propagation channels. Receiver-side inputs are formed via pilot-aided LS estimation and 2-D time–frequency interpolation, while ground-truth labels are obtained from the corresponding perfect channel responses.

Validation confirms broad coverage across SNR, delay spread, and Doppler shift, with balanced representation of TDL profiles. Input–label consistency analysis (correlation and NMSE) shows that the dataset captures both typical and extreme propagation conditions, and the binned trends versus SNR, delay spread, and Doppler exhibit physically consistent behavior. Qualitative 2-D/3-D visualizations further illustrate the channel structure and how mismatch increases under low SNR, high mobility, and large delay spreads.

In addition to statistical validation, a benchmark model was evaluated to establish baseline performance for learning-based channel estimation. The results demonstrated that a lightweight CNN trained on the ChanEst dataset consistently outperformed the LS estimator, achieving an average NMSE gain of 2.25 dB across the test set. While deliberately kept simple and not optimized for state-of-the-art accuracy, to encourage future architectural innovation, this reference model confirms that the dataset contains learnable, physically consistent representations of complex 6G channel impairments.

The current release is limited to OFDM-based systems and, therefore, does not include alternative pilot configurations or waveforms. Future extensions of the ChanEst framework will therefore incorporate additional waveforms, such as Orthogonal Time Frequency Space (OTFS), alongside the evaluation of state-of-the-art DL models. These enhancements will further improve the realism and flexibility of the dataset and enable broader benchmarking of deep learning techniques for next-generation wireless systems.

The ChanEst dataset is publicly released in MATLAB (.mat) and HDF5 (.h5) formats with per-sample metadata to support reproducible research and controlled evaluation. The dataset is available on Mendeley Data [23], and the codebase is available on GitHub, enabling researchers to regenerate and reconfigure the dataset and develop more advanced models. By providing a transparent and configurable dataset pipeline and baseline model, ChanEst aims to facilitate fair benchmarking, reproducibility, and accelerated research in deep learning–based channel estimation for future wireless networks.

Author Contributions: Conceptualization, O.O.; methodology, O.O.; software, O.O.; validation, O.O., X.D., and R.S.; formal analysis, D.J. and O.S.; investigation, O.O.; resources, O.O.; writing—original draft preparation, O.O.; writing—review and editing, O.S. and D.J.; supervision, X.D. and R.S.; project administration, X.D. and R.S. All authors have read and agreed to the published version of the manuscript.

Funding: This research received no external funding.

Data Availability Statement: The ChanEst dataset is publicly available on Mendeley Data (DOI: 10.17632/8w3zjj8hzc.1), and the corresponding codebase for regeneration and benchmarking is available on GitHub (https://github.com/obydelion/ChanEst-Dataset-Generation (accessed on 20 February 2026)).

Conflicts of Interest: The authors declare no conflicts of interest.

References

1. Saad, W.; Bennis, M.; Chen, M. A Vision of 6G Wireless Systems: Applications, Trends, Technologies, and Open Research Problems. *IEEE Netw.* **2020**, *34*, 134–142. [CrossRef]
2. Okoyeigbo, O.; Deng, X.; Sheriff, R.; Imoize, A.L.; Shobayo, O.; Ibhaze, A.E. CNN-Based Channel Estimation for Extreme Scenarios in 6G and Beyond. In *Proceedings of the 2025 International Conference on Smart Applications, Communications and Networking (SmartNets)*; IEEE: New York, NY, USA, 2025; pp. 1–6. [CrossRef]
3. Ye, H.; Li, G.Y.; Juang, B.-H. Power of Deep Learning for Channel Estimation and Signal Detection in OFDM Systems. *IEEE Wirel. Commun. Lett.* **2018**, *7*, 114–117. [CrossRef]
4. Liu, F.; Zhang, J.; Jiang, P.; Wen, C.-K.; Jin, S. CE-ViT: A Robust Channel Estimator Based on Vision Transformer for OFDM Systems. In *Proceedings of the GLOBECOM 2023—2023 IEEE Global Communications Conference*; IEEE: New York, NY, USA, 2023; pp. 4798–4803. [CrossRef]
5. Lagona, L.; Vakilifard, M.; Bockelmann, C.; Dekorsy, A. Transformer-Based Pilot-to-Prediction for Frequency-Selective Channels in OFDM Systems. *IEEE Wirel. Commun. Lett.* **2026**, *15*, 310–314. [CrossRef]
6. O'shea, T.; Hoydis, J. An Introduction to Deep Learning for the Physical Layer. *IEEE Trans. Cogn. Commun. Netw.* **2017**, *3*, 563. [CrossRef]
7. Lv, C.; Luo, Z. Deep Learning for Channel Estimation in Physical Layer Wireless Communications: Fundamental, Methods, and Challenges. *Electronics* **2023**, *12*, 4965. [CrossRef]
8. Fischione, C.; Chafii, M.; Deng, Y.; Erol-Kantarci, M. Data Sets for Machine Learning in Wireless Communications and Networks. *IEEE Commun. Mag.* **2023**, *61*, 80–81. [CrossRef]
9. Karim Gizzini, A.; Chafii, M.; Nimr, A.; Shubair, R.M.; Fettweis, G. CNN Aided Weighted Interpolation for Channel Estimation in Vehicular Communications. *IEEE Trans. Veh. Technol.* **2021**, *70*, 12796–12811. [CrossRef]
10. Cui, Z.; Zhang, P.; Pollin, S. 6G Wireless Communications in 7–24 GHz Band: Opportunities, Techniques, and Challenges. In Proceedings of the 2025 IEEE International Symposium on Dynamic Spectrum Access Networks (DySPAN), London, UK, 12–15 May 2025. [CrossRef]
11. Miao, H.; Zhang, J.; Tang, P.; Zhen, Q.; Meng, J.; Liu, X.; Liu, E.; Liu, P.; Tian, L.; Liu, G. 6G New Mid-Band/FR3 (6–24 GHz): Channel Measurement, Characteristics and Modeling. *IEEE Open J. Commun. Soc.* **2025**, *6*, 9942–9960. [CrossRef]
12. Ju, H.; Zhang, H.; Li, L.; Li, X.; Dong, B. A comparative study of deep learning and iterative algorithms for joint channel estimation and signal detection in OFDM systems. *Signal Process.* **2024**, *223*, 109554. [CrossRef]
13. Testolina, P.; Polese, M.; Melodia, T. Sharing Spectrum and Services in the 7–24 GHz Upper Midband. *IEEE Commun. Mag.* **2024**, *62*, 170–177. [CrossRef]
14. Alkhateeb, A. DeepMIMO: A Generic Deep Learning Dataset for Millimeter Wave and Massive MIMO Applications. 2019. Available online: http://arxiv.org/abs/1902.06435 (accessed on 30 January 2025).

15. Klautau, A.; De Oliveira, A.; Trindade, I.P.; Alves, W. Generating Mimo Channels for 6G Virtual Worlds Using Ray-Tracing Simulations. In Proceedings of the 2021 IEEE Statistical Signal Processing Workshop (SSP), Rio de Janeiro, Brazil, 11–14 July 2021. [CrossRef]
16. Oliveira, A.; Bastos, F.; Trindade, I.; Frazao, W.; Nascimento, A.; Gomes, D.; Muller, F.; Klautau, A. Simulation of machine learning-based 6G systems in virtual worlds. *ITU J. Future Evol. Technol.* **2021**, *2*, 113–123. [CrossRef]
17. Li, B.; Zheng, Q.; Tian, X.; Yang, M.; Gui, G.; Jiang, W.; Lei, H.; Jiang, J.; Shu, F.; Elhanashi, A.; et al. A Survey of Artificial Intelligence Enabled Channel Estimation Methods: Recent Advance, Performance, and Outlook. *Artif. Intell. Rev.* **2025**, *58*, 187. [CrossRef]
18. Catak, F.O.; Kuzlu, M.; Catak, E.; Cali, U.; Guler, O. Defensive Distillation-Based Adversarial Attack Mitigation Method for Channel Estimation Using Deep Learning Models in Next-Generation Wireless Networks. *IEEE Access* **2022**, *10*, 98191–98203. [CrossRef]
19. Belgiovine, M.; Sankhe, K.; Bocanegra, C.; Roy, D.; Chowdhury, K.R. Deep Learning at the Edge for Channel Estimation in Beyond-5G Massive MIMO. *IEEE Wirel. Commun.* **2021**, *28*, 19–25. [CrossRef]
20. Zhao, H. AI and Machine Learning in 5G. The ITU Challenge 2020. Available online: https://s41721.pcdn.co/wp-content/uploads/2021/06/En-AI-and-ML-for-5G.pdf (accessed on 29 January 2026).
21. Okoyeigbo, O.; Deng, X.; Imoize, A.L.; Shobayo, O. OTFS: A Potential Waveform for Space–Air–Ground Integrated Networks in 6G and Beyond. *Telecom* **2025**, *6*, 19. [CrossRef]
22. Longjohn, R.; Kelly, M.; Singh, S.; Smyth, P. Benchmark Data Repositories for Better Benchmarking. *Adv. Neural Inf. Process. Syst.* **2024**, *37*, 86435–86457. [CrossRef]
23. Okoyeigbo, O.; Sheriff, R.; Deng, X.; Shobayo, O.; Jeremiah, D. ChanEst Dataset for Deep Learning-Based 6G Channel Estimation. *Mendeley Data*, Version 1; 2026. [CrossRef]
24. Kim, W.; Ahn, Y.; Kim, J.; Shim, B. Towards deep learning-aided wireless channel estimation and channel state information feedback for 6G. *J. Commun. Netw.* **2023**, *25*, 61–75. [CrossRef]
25. *3GPP TR 38.901*; Study on Channel Model for Frequencies from 0.5 to 100 GHz; version 18.0.0, Release 18. 3GPP: Sophia Antipolis, France, 2024.
26. *3GPP TS 38.211*; NR; Physical Channels and Modulation; version 19.1.0, Release 19. 3GPP: Sophia Antipolis, France, 2025.
27. *3GPP TS 38.214*; NR; Physical Layer Procedures for Data; version 17.14.0, Release 17. 3GPP: Sophia Antipolis, France, 2025.
28. Rappaport, T.S.; Humphreys, T.E.; Nie, S. Spectrum opportunities for the wireless future: From direct-to-device satellite applications to 6G cellular. *npj Wirel. Technol.* **2025**, *1*, 8. [CrossRef]